

Scalable Polar Code Construction for Successive Cancellation List Decoding: A Graph Neural Network-Based Approach

Yun Liao, *Graduate Student Member, IEEE*,

Seyyed Ali Hashemi, *Member, IEEE*, Hengjie Yang, *Graduate Student
Member, IEEE*, and John M. Cioffi, *Life Fellow, IEEE*

Abstract

While constructing polar codes for successive-cancellation decoding can be implemented efficiently by sorting the bit-channels, finding optimal polar-code constructions for the successive-cancellation list (SCL) decoding in an efficient and scalable manner still awaits investigation. This paper proposes a graph neural network (GNN)-based reinforcement learning algorithm, named the *iterative message-passing (IMP)* algorithm, to solve the polar-code construction problem for SCL decoding. The algorithm operates only on the local structure of the graph induced by polar-code's generator matrix. The size of the IMP model is independent of the blocklength and the code rate, making it scalable to construct polar codes with long blocklengths. Moreover, a single trained IMP model can be directly applied to a wide range of target blocklengths, code rates, and channel conditions, and corresponding polar codes can be generated without separate training. Numerical experiments show that the IMP algorithm finds polar-code constructions that significantly outperform the classical constructions under cyclic-redundancy-check-aided SCL (CA-SCL) decoding. Compared to other learning-based construction methods tailored to SCL/CA-SCL decoding, the IMP algorithm constructs polar codes with comparable or lower frame error rates, while reducing the training complexity significantly by eliminating the need of separate training at each target blocklength, code rate, and channel condition.

Yun Liao and John M. Cioffi are with the Department of Electrical Engineering, Stanford University, Stanford, CA 94305, USA (email: yunliao@stanford.edu; cioffi@stanford.edu).

Seyyed Ali Hashemi is with Qualcomm Technologies, Inc., Santa Clara, CA 95051, USA (email: hashemi@qti.qualcomm.com).

Hengjie Yang is with the Department of Electrical and Computer Engineering, University of California at Los Angeles, CA 90095 USA (email: hengjie.yang@ucla.edu).

Index Terms

Graph neural networks, polar-code design, reinforcement learning, successive-cancellation list decoding.

I. INTRODUCTION

Polar codes, originally introduced by Arikan in [1], have attracted wide interests from both academia and industry because they achieve the capacity of any binary-input memoryless symmetric channels under the successive-cancellation (SC) decoding. Recently, the 5G standard adopted polar codes for use in the control channel, where relatively short blocklength codes are required [2]. While the original polar code design for the SC decoding is capacity-achieving as the code blocklength tends toward infinity, the error-correction performance of SC decoding is unsatisfactory in the short-blocklength regime. Some variants of the SC decoding, such as the SC list (SCL) decoding aided with a cyclic redundancy check (CRC) [3], have been proposed to further improve the decoding performance of polar codes with short blocklengths.

The polar encoding process divides the source vector into two sets, the non-frozen set and the frozen set. The non-frozen set carries the message, while the frozen set carries predefined values known to the decoder. The source vector is then encoded with the polar generator matrix to produce a polar codeword. The polar-code construction problem is to design the frozen set under a given channel condition and a given decoding algorithm such that the frame error rate is minimized.

In recent years, researchers have proposed multiple techniques to construct polar codes tailored for the SC decoding. Some important examples include the use of the Bhattacharyya parameter and its variants [1], [4], methods based on density evolution [5], [6], Gaussian approximation of density evolution [7], channel upgrading/downgrading techniques [8] for general symmetric binary-input memoryless channels, and Monte-Carlo-based bit-channel selection algorithm [9] that handles general channel conditions. In [10], [11], a universal partial ordering of the reliability of the bit-channels was discovered, which gives rise to a polar-code construction algorithm whose complexity is sublinear in blocklength [12]. A β -expansion construction method [13] was also proposed based on this universal partial order.

All aforementioned construction techniques are predicated on the observation that the information bits should be transmitted over the most reliable bit-channels to achieve the optimal error-correction performance under SC decoding. However, experiments have shown that when SCL or

CRC-aided SCL (CA-SCL) decoding is employed, the polar codes constructed by selecting the most reliable bit-channels do not necessarily result in the best error-correction performance [14]. In fact, due to the nature of SCL decoding, there may not even exist a single reliability order of bit-channels that captures the optimal polar code constructions for arbitrary code rates. In fact, for a given channel, rigorous analysis of the error-correction performance and the optimal code construction under SCL decoding still remain an open problem. Nevertheless, some important theoretical breakthroughs have been made toward understanding polar codes. In [15], Yao *et al.* developed a deterministic recursive algorithm to compute the weight enumerating function of polar codes. Recently, Coşkun and Pfister [16] analyzed the list size required for the SCL decoder in order to achieve the maximum likelihood decoding performance. Several methods, including special CRC designs [17], [18], data-dependent frozen bits [19], and altering construction patterns [20]–[22] have been proposed to design better polar codes for SCL decoding. A log-likelihood ratio (LLR)-evolution-based construction method that swaps vulnerable non-frozen bit-channels with strong frozen bit-channels was proposed in [20] for belief propagation (BP) decoding of polar codes, where the modified constructions showed improvement under SCL decoding. In [21], the polar codes' minimum Hamming distance was improved by excluding bits corresponding to low-Hamming-weight rows in the generator matrix, while [22] improved the Hamming distance of polar codes by dynamically assigning frozen bits.

Recently, artificial-intelligence (AI) techniques have also evolved as promising tools to construct polar codes [23]–[26]. A deep-learning-based polar code construction method for BP decoding was introduced in [25]. [23] and [24] proposed to use genetic algorithms to construct polar codes for SCL decoding. In [26], a reinforcement-learning (RL)-based algorithm was proposed to construct polar codes for the SCL decoding, which reduced the training sample complexity compared to the genetic algorithms. However, all of these methods require separate training for each design scenario, even when there is only a minimal change in code rate and/or the target channel condition. In other words, these AI-based algorithms provide satisfying polar-code constructions only for the trained cases, and cannot be generalized to other code design tasks with different parameters. Moreover, the training complexity becomes prohibitively high as the blocklength increases or as the frame error rate (FER) decreases, making these algorithms not suitable for designing polar codes of long blocklengths.

As its main contributions, this paper proposes a graph neural network (GNN)-based algorithm for finding polar-code constructions tailored for the CA-SCL decoding, namely, the *itera-*

tive message-passing (IMP) algorithm on a polar-code-construction message-passing (PCCMP) graph, in which GNNs are trained to build the frozen-bit set based on the target channel condition and code rate iteratively. The fact that all algorithmic operations in the algorithm are local on the PCCMP graph guarantees that the GNN model complexity is independent of the blocklength and code rate, and a trained IMP model under one code-design requirement is directly applicable to different design requirements such as different blocklengths, code rates, and channel conditions. In other words, the IMP model is naturally scalable to polar codes with long blocklengths and can be generalized to design requirements that are not seen during training. Experiments show that the polar codes found by the IMP algorithm significantly outperform the classical constructions in [8] under the CA-SCL decoding, and achieve similar or lower FERs compared to existing construction methods tailored for CA-SCL decoding with significantly lower training complexity. Experiments verify the IMP algorithm’s generalization capability by applying a single trained IMP model directly to generate polar codes with different channel signal-to-noise ratios (SNRs) and blocklengths.

The remainder of this paper is organized as follows. Section II briefly introduces the preliminaries of polar codes, GNNs, and RL systems. Section III describes the design of the PCCMP graph and the IMP algorithm. The GNN model and the training process are detailed in Section IV. Section V presents experiment results and observations. Finally, Section VI concludes the paper.

II. PRELIMINARIES

A. Notation

Throughout the paper, denote by $[n] \triangleq \{0, 1, \dots, n-1\}$. A length- n column vector is denoted by a bold lowercase letter, e.g., $\mathbf{x} \in \mathbb{R}^n$, in which the i -th element is written as $x[i]$, $i \in [n]$; an $n \times m$ matrix is denoted by a bold uppercase letter, e.g., $\mathbf{X} \in \mathbb{R}^{n \times m}$, in which the (i, j) -th entry of matrix \mathbf{X} is given by $X[i, j]$, $i \in [n], j \in [m]$. Let $(\cdot)^\top$ represent the transpose of a vector or a matrix, $[\mathbf{x}_1^\top, \mathbf{x}_2^\top]^\top$ the vertical concatenation of \mathbf{x}_1 and \mathbf{x}_2 , and $\|\mathbf{x}\|_2$ the ℓ_2 norm of a vector \mathbf{x} . Sets are denoted by calligraphic letters, e.g., \mathcal{I} , and $|\cdot|$ represents the cardinality of a set. In the description of graphs and GNNs, a directed edge from node u to node v is represented by (u, v) , and the superscript i in $(\cdot)^{(i)}$ denotes the i -th message passing iteration. The CRC (generator) polynomial is represented in hexadecimal, in which the corresponding binary coefficients are written from the highest to the lowest order. The coefficient of the highest order bit is omitted

because it is always 1. For instance, the degree-4 CRC polynomial $x^4 + (x + 1)$ is written as 0x3.

B. Polar Codes and SC-Based Decoding

Let $\mathcal{P}(N, K, m)$ denote a polar code of length $N = 2^n$, rate $R = (K - m)/N$, and m bits of CRC, where $n \in \mathbb{N}$, $0 \leq m < K < N$. A codeword $\mathbf{c} \in \mathbb{F}_2^N$ in $\mathcal{P}(N, K, m)$ is obtained by applying a linear transformation $\tilde{\mathbf{G}}_n$ to the source vector $\mathbf{u} = (u[0], u[1], \dots, u[N - 1])^\top$ as $\mathbf{c} = \mathbf{u}^\top \tilde{\mathbf{G}}_n$, in which the generator matrix $\tilde{\mathbf{G}}_n$ is constructed from the Arıkan's polarization kernel \mathbf{G} as $\tilde{\mathbf{G}}_n = \mathbf{G}^{\otimes n} = \begin{bmatrix} 1 & 0 \\ 1 & 1 \end{bmatrix}^{\otimes n}$, where $\mathbf{G}^{\otimes n}$ is the n -th Kronecker power of \mathbf{G} [1]. The extended input vector \mathbf{u} contains a set \mathcal{F} of $(N - K)$ frozen bits and a set \mathcal{I} of K non-frozen bits. The positions and values of the frozen bits are known to both the encoder and the decoder, and their values are commonly set to zero. The K non-frozen bits include m CRC bits and $(K - m)$ information bits. If no CRC is used, $m = 0$. The *construction* of a polar code $\mathcal{P}(N, K, m)$ is to select the positions of the $(N - K)$ frozen bits and the positions of the m CRC bits for a specific design channel condition. For simplicity, in this paper, the CRC bits, if any, are appended after the $(K - m)$ information bits. Then, the construction problem is reduced to choosing $(N - K)$ out of N positions as frozen bits. Moreover, this work considers quadrature phase-shift keying (QPSK) modulation for an additive white Gaussian noise (AWGN) channel, in which the SNR is defined as $\gamma \triangleq 10 \log_{10}(E_s/N_0)$ dB, where E_s denotes energy per transmitted symbol and N_0 denotes the one-sided power spectral density of the AWGN.

The SC decoding and its variants are sequential decoding algorithms, in which source bit $u[k]$ is decoded based on the entire received signal as well as the previous k decoded source bits. The SC decoder decodes each bit by assuming all previous source bits are decoded correctly, which is prone to cascading decoding errors. The SCL decoder improves the decoding performance of SC decoding by keeping up to L most likely decoding paths in parallel [3], in which L is referred to as the list size. When the decoding process terminates, one codeword is selected from the candidate list as the decoding output either based on the likelihood, which is called the pure SCL decoding, or by using a CRC verification, which is referred to as the CA-SCL decoding.

C. Basic Concepts in GNNs

GNNs are neural models that can be directly applied to input graphs $\mathcal{G}(\mathcal{V}, \mathcal{E})$, in which \mathcal{V} represents the set of nodes in the graph, and \mathcal{E} represents the set of directed edges, e.g., for a

pair of nodes $u, v \in \mathcal{V}$, $(u, v) \in \mathcal{E}$ if and only if there exists a directed edge in graph \mathcal{G} from u to v . The node features are denoted by a $d \times |\mathcal{V}|$ matrix \mathbf{X} , in which each column represents the d -dimensional local feature of a node in \mathcal{V} . A node embedding is a vector representation of a node, abstracted such that nodes with similar embeddings are expected to have similar local neighborhoods and features [27]. GNNs are efficient tools to generate such node embeddings, which can be readily applied to graph-related tasks, such as node selection, link prediction, and graph classification.

The defining feature of a GNN is the usage of neural message passing, in which vector messages are exchanged between nodes and are updated using neural networks (NNs) [28]. During the i -th message-passing iteration in a GNN, a hidden embedding $\mathbf{h}_u^{(i)}$, corresponding to each node $u \in \mathcal{V}$, is updated according to information aggregated from u 's in-neighborhood $\mathcal{N}(u) \triangleq \{w | (w, u) \in \mathcal{E}\}$. A general message passing update rule at iteration i can be expressed as

$$\mathbf{h}_{\mathcal{N}(u)}^{(i+1)} = \text{AGG}^{(i)} \left(\{\mathbf{h}_w^{(i)}, \forall w \in \mathcal{N}(u)\} \right), \quad (1)$$

$$\mathbf{h}_u^{(i+1)} = \text{UP}^{(i)} \left(\mathbf{h}_u^{(i)}, \mathbf{h}_{\mathcal{N}(u)}^{(i+1)} \right), \quad \forall u \in \mathcal{V}, \quad (2)$$

where $\text{AGG}^{(i)}$ defines the aggregation operation on the set of incoming messages sent to a node from its neighbors during iteration i (e.g., summation or averaging of incoming messages), and $\text{UP}^{(i)}$ specifies the update operation during iteration i . Both AGG and UP are arbitrary differentiable functions. Note that since the AGG function takes a set as input, GNNs defined in this way are permutation equivariant by design. The initial embeddings at $i = 0$ are set to $\mathbf{h}_u^{(0)} = \mathbf{x}_u$, $\forall u \in \mathcal{V}$, where $\mathbf{x}_u \in \mathbb{R}^d$ is the column vector in \mathbf{X} that corresponds to node u . The final node representations are outputs $\mathbf{h}_u^{(M)}$, $\forall u \in \mathcal{V}$, at the final iteration, where the hyper-parameter M denotes the maximum number of message-passing iterations.

Heterogeneous GNNs [29] are used to handle the tasks in which the input graphs include various types of nodes and edges, and the types of messages passed along different types of edges are different. A heterogeneous GNN applies the update rules (1) and (2) to each message type separately, where a message type mt describes the relationship captured by the (directed) edge between a pair of nodes. For example, the message type of the edge “cat $\xrightarrow{\text{is a}}$ mammal” can be viewed as $\text{mt} = \text{“is a”}$ or “subset”. The final updated message at each node aggregates the updates from all message types.

Formally, the in-neighborhood of node u with message type mt is defined by

$$\mathcal{N}_{\text{mt}}(u) \triangleq \{w \in \mathcal{N}(u) | \mathbb{T}_{\text{msg}}((w, u)) = \text{mt}\}, \quad (3)$$

where the function $\mathbb{T}_{\text{msg}}((w, u))$ gives the message type of edge $(w, u) \in \mathcal{E}$. Define $\mathcal{MT}(u) \triangleq \{\text{mt} | \mathcal{N}_{\text{mt}}(u) \neq \emptyset\}$ as the set of message types that are sent to node u . The update rule at each node u is split into the following three steps:

Step 1): Node u aggregates messages of type mt from $\mathcal{N}_{\text{mt}}(u)$ separately for every $\text{mt} \in \mathcal{MT}(u)$:

$$\mathbf{h}_{\mathcal{N}_{\text{mt}}(u)}^{(i+1)} = \text{AGG}_{\text{mt}}^{(i)} \left(\{\mathbf{h}_w^{(i)} | w \in \mathcal{N}_{\text{mt}}(u)\} \right), \quad (4)$$

where $\text{AGG}_{\text{mt}}^{(i)}$ is the aggregation operator for message type mt during iteration i .

Step 2): Node u calculates the update from each message type $\text{mt} \in \mathcal{MT}(u)$ as

$$\mathbf{h}_{u, \text{mt}}^{(i+1)} = \text{UP}_{\text{mt}}^{(i)} \left(\mathbf{h}_u^{(i)}, \mathbf{h}_{\mathcal{N}_{\text{mt}}(u)}^{(i+1)} \right), \quad (5)$$

where $\text{UP}_{\text{mt}}^{(i)}$ denotes the update operation for message type mt during iteration i .

Step 3): Node u aggregates the update given by each message type to obtain the final update as

$$\mathbf{h}_u^{(i+1)} = \text{AGG}_{\mathbb{T}_n(u)}^{(i)} \left(\left\{ \mathbf{h}_{u, \text{mt}}^{(i+1)} | \text{mt} \in \mathcal{MT}(u) \right\} \right), \quad (6)$$

in which $\mathbb{T}_n(u)$ gives the node type of u , and the aggregation function $\text{AGG}_{\mathbb{T}_n(u)}^{(i)}$ can be different for different node types. This work uses the same aggregation operation for all node types to simplify the model, i.e.,

$$\mathbf{h}_u^{(i+1)} = \text{AGG}^{(i)} \left(\left\{ \mathbf{h}_{u, \text{mt}}^{(i+1)} | \text{mt} \in \mathcal{MT}(u) \right\} \right), \quad \forall u \in \mathcal{V}. \quad (7)$$

Note that the aggregation operation $\text{AGG}^{(i)}$ can still be different for different iterations.

Since the message passing update rules (4)-(6) only operate on each node u 's local in-neighborhood and the same rule is applied to every node $u \in \mathcal{V}$ in the graph, a GNN defined in this way can be used directly on graphs of arbitrary sizes with arbitrary structures. The model complexity, on the other hand, only depends on the complexity of the UP and AGG functions, the number of iterations M , and the number of message types if the graph is heterogeneous, and is independent of the input graph size. More importantly, the local processing feature of GNN models makes the generalization over graphs possible: a well-designed GNN can be trained on small graphs and then be applied to significantly larger graphs with similar properties or local structures directly.

D. Basics of a RL System and Deep Q-learning (DQL)

RL is a type of machine learning technique that enables an agent to learn in an interactive environment by trial and error using feedback from its own actions and experiences. RL techniques are shown to be particularly powerful for a Markov decision process (MDP) environment, in which the environment's state transition and feedback to the agent (reward) are conditionally independent of the agent's interaction history with the environment given the current environment state and the agent's action. A typical RL setup for a MDP environment is defined by the following key elements:

- a set \mathcal{S} representing **states** of the environment;
- an **action space** $\mathcal{A}(s)$ that specifies the set of actions that the agent can take at state s ;
- a **transition rule** $\Pr(s'|s, a)$, which is the probability of transitioning to state $s' \in \mathcal{S}$ at the next time step given that the agent takes action $a \in \mathcal{A}(s)$ at the current state s . The transition probability may be unknown to the agent;
- an immediate **reward** function $r(s, a, s')$ that determines the agent's received reward when the agent takes action a at state s and the environment transitions to state s' . The reward function can be stochastic.

The interaction between the agent and the environment is an iterative process. At each time t , the agent senses the environment's state s_t and chooses an action a_t from $\mathcal{A}(s_t)$. The environment, stimulated by the agent's action, changes its state to s_{t+1} and sends reward r_{t+1} back to the agent. The agent accumulates the rewards as this interaction continues. The goal of the agent is to learn a **policy** $\pi : \mathcal{S} \times \mathcal{A} \rightarrow [0, 1]$ with $\pi(a|s) = \Pr(A_t = a | S_t = s)$ such that the expected long-term **return** R is maximized. Here, the return is defined as $R = \sum_{t=0}^T \beta^t r_{t+1}$, where $\beta \in [0, 1]$ is the discount factor that describes how much the agent weights the future reward, and T denotes the game's termination time. If a policy π is deterministic, i.e., for all $s \in \mathcal{S}$, $\pi(a|s) = 1$ for some action a and $\pi(a'|s) = 0$ for all $a' \neq a$, the policy π is also written as $\pi(s) = a$ for simplicity.

III. POLAR-CODE CONSTRUCTION BASED ON MESSAGE PASSING GRAPH

The generalization capability of GNNs over various graph sizes and over embedded messages motivates the mapping of the polar-code construction problem to a graph-related task, in which the input graphs are designed such that the nodes' local structures are likely to reflect the importance or reliability of the bit-channels. This section presents the design of the input graphs

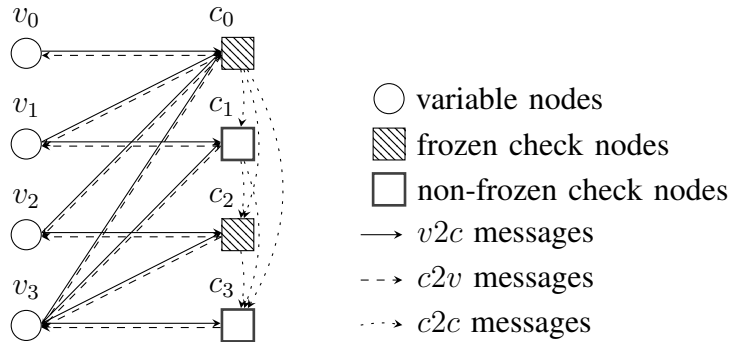


Fig. 1: PCCMP graph for $\mathcal{P}(4, 2, \cdot)$ with $\mathcal{I} = \{1, 3\}$ and $\mathcal{F} = \{0, 2\}$.

and the GNN-based polar-code construction algorithm, which does not rely on the reliability ordering, and can be easily applied to large N and K without increasing the model complexity.

A. Polar-Code-Construction Message-Passing (PCCMP) Graph

In analogy with the construction of Tanner graphs for BP decoding, a polar-code-construction message-passing (PCCMP) graph $\mathcal{G}_N(\mathcal{V}_N, \mathcal{E}_N)$ that assists the construction of $\mathcal{P}(N, K, m)$ for CA-SCL decoding is generated as follows. First, a bipartite graph is constructed with N variable nodes $\mathcal{W}_N \triangleq \{v_0, \dots, v_{N-1}\}$ and N check nodes¹ $\mathcal{C}_N \triangleq \{c_0, \dots, c_{N-1}\}$. Directed edges (v_i, c_j) and (c_j, v_i) exist if and only if $\tilde{G}_n[i, j] = 1$. In addition, each c_{j_1} is connected to c_{j_2} for all $0 \leq j_1 < j_2 \leq N - 1$ by directed edges. The rationale for the edges between check nodes is explained in Remark 3.

The node type of any variable node $u \in \mathcal{W}_N$ is $\mathbb{T}_n(u) = \text{V}$. The node type of a check node c_i , $i \in [N]$ is

$$\mathbb{T}_n(c_i) = \begin{cases} \text{F}, & \text{if } c_i \text{ is a frozen node,} \\ \text{I}, & \text{if } c_i \text{ is a non-frozen node.} \end{cases} \quad (8)$$

Every polar-code construction has a one-to-one mapping to the types of the check nodes' types in the PCCMP graph as follows:

$$\mathbb{T}_n(c_i) = \text{I} \Leftrightarrow i \in \mathcal{I}, \quad \mathbb{T}_n(c_i) = \text{F} \Leftrightarrow i \in \mathcal{F}, \quad \forall i \in [N]. \quad (9)$$

¹The term *check node* is slightly abused here. Only nodes c_i , $i \in \mathcal{F}$ are real check nodes in BP decoding and have predetermined values. All other nodes c_i represent the non-frozen bits and need to be recovered.

The message types in the PCCMP graph are defined as

$$\mathbb{T}_{\text{msg}}((c_j, v_i)) = c2v; \quad \mathbb{T}_{\text{msg}}((v_i, c_j)) = v2c; \quad \mathbb{T}_{\text{msg}}((c_i, c_j)) = c2c. \quad (10)$$

Fig. 1 illustrates the PCCMP graph for $\mathcal{P}(4, 2, \cdot)$ with $\mathcal{I} = \{1, 3\}$ and $\mathcal{F} = \{0, 2\}$.

Remark 1: The structure (i.e., nodes and connections) of the PCCMP graph for $\mathcal{P}(N, K, m)$ as well as the edge types is completely determined by N , and is independent of the code construction, i.e., the non-frozen set \mathcal{I} and frozen set \mathcal{F} . Similar construction-independent feature can be observed in the factor graph representations of SC decoding [1], in which different constructions share the same factor graph that differ only in processing functions.

B. Iterative Message-Passing (IMP) Algorithm

The proposed polar-code construction algorithm, named *IMP* algorithm, iterates between a message passing phase on the PCCMP graph and a local post-processing procedure. Algorithm 1 provides the skeleton of the IMP algorithm, in which all functions are specified in Section IV-A. The IMP algorithm initializes all check nodes as non-frozen, and changes one non-frozen check node to frozen in each step. The construction of polar code $\mathcal{P}(N, K, m)$ is therefore obtained in $N - K$ steps.

During the message passing phase in each step, the hidden embedding of each node $u \in \mathcal{V}_N$ is initialized as

$$\mathbf{h}_u^{(0)} = \text{INIT}_{\mathbb{T}_n(u)}(\mathbf{x}_u), \quad \forall u \in \mathcal{V}_N, \quad (11)$$

where \mathbf{x}_u represents the initial information at node u and the initialization operators $\text{INIT}_{\mathbb{T}_n(u)}(\cdot)$ can be different for different node types. Each node then collects and processes the incoming messages by their message types, and then updates its embedding as in (5) and (7). Since the PCCMP graph is constructed such that each variable node is only connected to check nodes, and each check node is connected to both variable nodes and check nodes, the message flow on a PCCMP graph in M message passing iterations can be abstracted as the diagram in Fig. 2, in which $\mathbf{h}_c^{(i)} = \{\mathbf{h}_{c_j}^{(i)} | j \in [N]\}$ and $\mathbf{h}_v^{(i)} = \{\mathbf{h}_{v_j}^{(i)} | j \in [N]\}$ represent the hidden embeddings of all check nodes and all variable nodes after i message passing iterations, respectively.

After the message passing phase, the global features of the hidden embeddings of the variable nodes and the check nodes are abstracted by the pooling operations $\text{POOL}_V(\cdot)$ and $\text{POOL}_C(\cdot)$, respectively, as

$$\tilde{\mathbf{h}}_v = \text{POOL}_V(\mathbf{h}_v^{(M)}); \quad \tilde{\mathbf{h}}_c = \text{POOL}_C(\mathbf{h}_c^{(M)}). \quad (12)$$

Algorithm 1 IMP Algorithm

Input: N, K ; initial information $\mathbf{x}_u, \forall u \in \mathcal{V}_N$; maximum message passing iterations M .

Output: Selected frozen set \mathcal{F} and nonfrozen set \mathcal{I} .

- 1: Initialize $\theta \leftarrow 1$; PCCMP graph \mathcal{G}_N , in which $\mathbb{T}_n(u) = \text{I}, \forall u \in \mathcal{C}_N$.
- 2: **for** step $t \leftarrow 1 : N - K$ **do**
- 3: Initialize $\mathbf{h}_u^{(0)} \leftarrow \text{INIT}_{\mathbb{T}_n(u)}(\mathbf{x}_u), \forall u \in \mathcal{V}_N$. ▷ message passing phase
- 4: **for** $i \leftarrow 0 : M - 1$ **do**
- 5: **for** $u \in \mathcal{V}_N$ **do**
- 6: **for** $\text{mt} \in \mathcal{MT}(u)$ **do**
- 7: $\mathbf{h}_{\mathcal{N}_{\text{mt}}(u)}^{(i+1)} \leftarrow \text{AGG}_{\text{mt}}^{(i)}\left(\left\{\mathbf{h}_w^{(i)} \mid w \in \mathcal{N}_{\text{mt}}(u)\right\}\right)$;
- 8: $\mathbf{h}_{u,\text{mt}}^{(i+1)} \leftarrow \text{UP}_{\text{mt}}^{(i)}\left(\mathbf{h}_u^{(i)}, \mathbf{h}_{\mathcal{N}_{\text{mt}}(u)}^{(i+1)}\right)$;
- 9: **end for**
- 10: $\mathbf{h}_u^{(i+1)} \leftarrow \text{AGG}^{(i)}\left(\left\{\mathbf{h}_{u,\text{mt}}^{(i+1)} \mid \text{mt} \in \mathcal{MT}(u)\right\}\right)$;
- 11: **end for**
- 12: **end for**
- 13: Compute $\tilde{\mathbf{h}}_v \leftarrow \text{POOL}_V\left(\mathbf{h}_{\mathcal{W}}^{(M)}\right)$; $\tilde{\mathbf{h}}_c \leftarrow \text{POOL}_C\left(\mathbf{h}_{\mathcal{C}}^{(M)}\right)$. ▷ post-processing phase
- 14: Each $c_j \in \mathcal{C}_N$ computes $z_j \leftarrow \text{POST}\left(\mathbf{h}_{c_j}^{(M)}, \tilde{\mathbf{h}}_v, \tilde{\mathbf{h}}_c, \theta\right), j \in [N]$.
- 15: Update \mathcal{G}_N by setting $\mathbb{T}_n(c_{j^*}) \leftarrow \text{F}$, where

$$j^* \leftarrow \arg \max_{\{j \in [N] \mid \mathbb{T}_n(c_j) = \text{I}\}} \{z_j\}.$$
- 16: $\theta \leftarrow \theta - \frac{1}{N-K}$.
- 17: **end for**
- 18: **return** $\mathcal{I} \leftarrow \{j \mid j \in [N], \mathbb{T}_n(c_j) = \text{I}\}$; $\mathcal{F} \leftarrow \{j \mid j \in [N], \mathbb{T}_n(c_j) = \text{F}\}$.

These global features are expected to provide high-level characterization about the graph structure and the underlying channel condition. Each check node c_j then applies a local post-processing operation $\text{POST}(\cdot)$ to its hidden embedding and the global features, and obtains a final scalar priority metric as

$$z_j = \text{POST}\left(\mathbf{h}_{c_j}^{(M)}, \tilde{\mathbf{h}}_v, \tilde{\mathbf{h}}_c, \theta\right), j \in [N], \quad (13)$$

where θ is an auxiliary parameter related to the number of remaining iterations to construct the target $\mathcal{P}(N, K, m)$. This work sets $\theta = 1 - \frac{t}{N-K} \in [0, 1]$ during iteration t of the IMP algorithm.

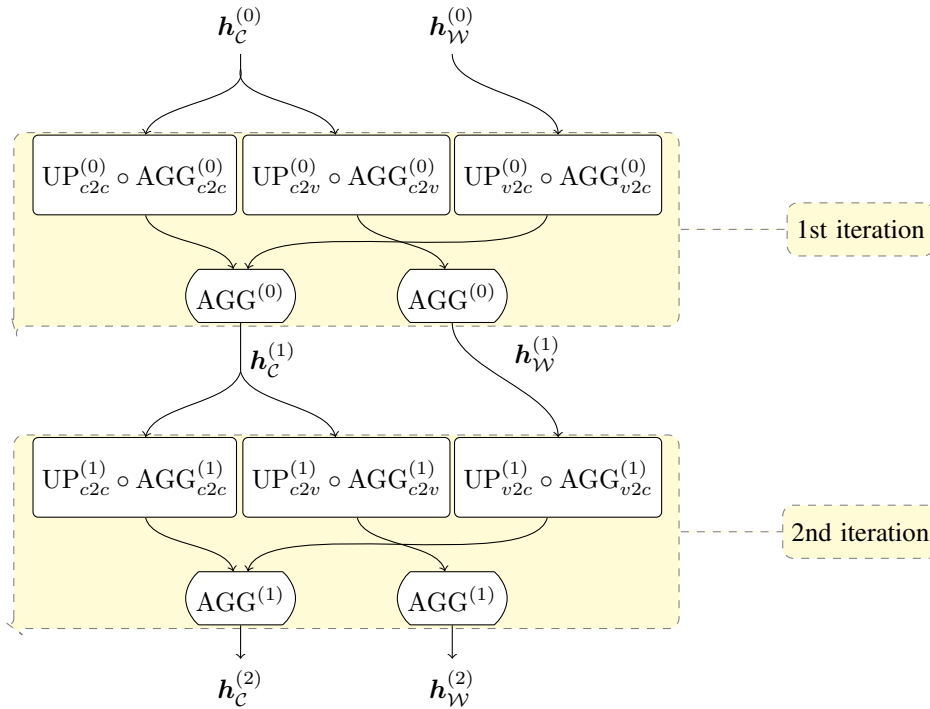


Fig. 2: Message passing operations on a PCCMP graph with $M = 2$.

Finally, the algorithm selects the non-frozen check node c_{j^*} with the largest priority metric z_{j^*} and changes it to frozen.

Remark 2: The auxiliary parameter θ is critical in the IMP algorithm because it allows the post-processing function $\text{POST}(\cdot)$ to return different priority metrics for different target code rates, even when the blocklength and the channel condition remain unchanged. These target-rate-dependent priority metrics make it possible for the IMP algorithm to produce polar-code constructions that do not depend on any global reliability ordering.

Remark 3: The edges connecting check nodes provide shortcuts on the PCCMP graph that allow each check node to receive messages directly from all of its preceding check nodes. In particular, each check node is aware of the number of frozen and non-frozen nodes that is decoded before it in CA-SCL decoding. Such information is expected to affect the check nodes' priority $\{z_j\}$ in (13) in the code constructions for CA-SCL decoding. Intuitively, in CA-SCL decoding, a reliable frozen bit can be helpful when there are many preceding non-frozen bits because it is likely to increase the advantage of the correct codeword's likelihood over the other candidate decoding outcomes. This influence is unique to SCL and CA-SCL decoding compared

to the SC decoding due to the maintenance of a candidate list in SCL and CA-SCL decoding.

Many existing polar-code construction methods for SC decoding can be viewed as special cases of the IMP algorithm. Appendix I shows a feasible mapping from the existing methods to the IMP algorithm and the corresponding design of the message processing functions for the IMP algorithm.

IV. DEEP Q-LEARNING FOR GRAPH-NEURAL-NETWORK-BASED IMP ALGORITHM

To exploit the full potential of the IMP algorithm, the initialization operations INIT_I and INIT_F , the update operations $\text{UP}_{\text{mt}}^{(i)}$, the post-processing operations POOL_C , POOL_V , and POST are all expressed as NNs. This section sketches the NN model design for the IMP algorithm, then formulates the IMP algorithm as a MDP, with which the NN model can be effectively learned by DQL. The training strategies for the IMP algorithm are also detailed.

A. GNN Model Design

1) *Initial local messages and initialization operations:* The initial local message at each node is set to scalars $x_{v_j} = \gamma$, and $x_{c_j} = \frac{j}{N}$ for $j \in [N]$, where γ denotes the SNR defined in Section II. The initialization operator concatenates a node-type embedding $\text{Emb}(\mathbb{T}_n(u)) \in \mathbb{R}^{d_{\text{emb}}}$ and an initial local-message embedding of length d_{init} . The node-type embedding $\text{Emb}(\mathbb{T}_n(u))$ is a lookup table that maps each node type to a trainable vector embedding. The initial local-message embeddings are generated by a single-layer fully-connected network with $\tanh(\cdot)$ activation. Formally, the initialization operator $\text{INIT}_{\mathbb{T}_n(u)}(\cdot)$ is given by

$$\text{INIT}_{\mathbb{T}_n(u)}(x_u) = \begin{cases} [\text{Emb}(\mathbb{T}_n(u))^\top, f_{\text{init},V}(x_u)^\top]^\top, & u \in \mathcal{W}_N, \\ [\text{Emb}(\mathbb{T}_n(u))^\top, f_{\text{init},C}(x_u)^\top]^\top, & u \in \mathcal{C}_N, \end{cases} \quad (14)$$

where

$$f_{\text{init},t}(x_u) = \tanh(\mathbf{w}_t^{\text{init}} \cdot x_u + \mathbf{b}_t^{\text{init}}) \in \mathbb{R}^{d_{\text{init}}}, \quad t = V, C, \quad (15)$$

where $\mathbf{w}_t^{\text{init}}, \mathbf{b}_t^{\text{init}} \in \mathbb{R}^{d_{\text{init}}}$ are trainable parameters. The initial embedding dimension of each node is $d^{(0)} = d_{\text{init}} + d_{\text{emb}}$. Note that the frozen check nodes and the non-frozen check nodes share the same NN model for the initial local-message embedding by design, and they are only different in the node-type embeddings.

2) *Neighborhood aggregation operations:* The mean-aggregation is adopted for both message types $c2v$ and $c2c$ in all iterations, i.e.,

$$\text{AGG}_{\text{mt}}^{(i)}(\{\mathbf{h}_w|w \in \mathcal{N}\}) = \frac{\sum_{w \in \mathcal{N}} \mathbf{h}_w}{|\mathcal{N}|}, \text{ mt} \in \{c2v, c2c\}, \forall i \in [M]. \quad (16)$$

The sum-aggregation is used by the message type $v2c$ as

$$\text{AGG}_{v2c}^{(i)}(\{\mathbf{h}_w|w \in \mathcal{N}\}) = \sum_{w \in \mathcal{N}} \mathbf{h}_w, \forall i \in [M]. \quad (17)$$

The rationale for such choices of aggregation operators is the following. The mean-aggregation only keeps the information of an average direction of the neighboring nodes' embedding, and the result does not scale up with the degree of the central node. This is desired for the PCCMP graph in general because the size of in-neighborhood $\mathcal{N}_{\text{mt}}(u)$ of each message type varies from 1 to N in the graph, and keeping aggregated messages in a similar scale helps stabilizing the training process. The aggregated message from $v2c$ edges, however, may be more helpful to the node-selection process if the degree information is included. This is because check nodes connecting to more variable nodes are more susceptible to noise, and thus would expect higher priority in the frozen-node selection process.

3) *Update operations:* The update operations in this work take the format of one convolutional layer in the GraphSAGE algorithm [30]:

$$\text{UP}_{\text{mt}}^{(i)}(\mathbf{h}_u, \mathbf{h}_{\mathcal{N}_{\text{mt}}(u)}) = \mathbf{W}_{\text{mt}}^{(i)} \cdot [\mathbf{h}_u^\top, \mathbf{h}_{\mathcal{N}_{\text{mt}}(u)}^\top]^\top + \mathbf{b}_{\text{mt}}^{(i)}, \text{ mt} \in \mathcal{MT}(u), \quad (18)$$

where $\mathbf{W}_{\text{mt}}^{(i)} \in \mathbb{R}^{d^{(i+1)} \times 2d^{(i)}}$, $\mathbf{b}_{\text{mt}}^{(i)} \in \mathbb{R}^{d^{(i+1)}}$.

4) *Local aggregation operations:* The local aggregation operators are given by

$$\text{AGG}^{(i)}(\{\mathbf{h}_{u,\text{mt}}|\text{mt} \in \mathcal{MT}(u)\}) = \text{ReLU}\left(\frac{\mathbf{s}_u}{\|\mathbf{s}_u\|_2}\right), i \in [M], \quad (19)$$

where $\mathbf{s}_u = \sum_{\text{mt} \in \mathcal{MT}(u)} \mathbf{h}_{u,\text{mt}}$ and $\text{ReLU}(\mathbf{x}) \triangleq \max(\mathbf{x}, \mathbf{0})$.

5) *Pooling operations:* The pooling operations for check nodes and variable nodes are defined, respectively, as

$$\text{POOL}_C(\mathbf{h}_C) \triangleq \tanh\left[\mathbf{W}_C^{\text{pool}} \cdot \left(\frac{1}{|\mathcal{C}|} \sum_{u \in \mathcal{C}} \mathbf{h}_u\right)\right], \quad (20)$$

$$\text{POOL}_V(\mathbf{h}_W) \triangleq \tanh\left[\mathbf{W}_V^{\text{pool}} \cdot \left(\frac{1}{|\mathcal{W}|} \sum_{u \in \mathcal{W}} \mathbf{h}_u\right)\right], \quad (21)$$

where $\mathbf{W}_C^{\text{pool}}, \mathbf{W}_V^{\text{pool}} \in \mathbb{R}^{d_{\text{pool}} \times d^{(M)}}$. The global features $\tilde{\mathbf{h}}_c$ and $\tilde{\mathbf{h}}_v$ are both vectors of length d_{pool} .

6) *Post processing*: A multilayer perceptron (MLP) with ReLU activation is used as the local post processing function applied to every check node c_j . The input to the MLP is the concatenation of $\mathbf{h}_{c_j}^{(M)}$, $\tilde{\mathbf{h}}_v$, $\tilde{\mathbf{h}}_c$, and θ . The output layer has a single unit with no (nonlinear) activation.

With the above specifications, all (trainable) parameters in the IMP model Θ include the node-type embeddings, and the weights and biases in the initial local-message embeddings, the update operations, the pooling operations, and the post processing MLP.

B. IMP-based Polar-Code Construction as a MDP

As suggested by Algorithm 1, the construction of $\mathcal{P}(N, K, m)$ requires $N - K$ iterations of selecting frozen bits in the IMP algorithm. The evolution of the IMP algorithm can be mapped to the following MDP environment defined on the PCCMP graphs:

- **State**: a state s_t is defined as the PCCMP graph at time t , i.e., $s_t = \mathcal{G}_{N,t}$, in which the set of nodes is denoted by $\mathcal{V}_{N,t} = \mathcal{W}_N \cup \mathcal{C}_{N,t}$. Define $\mathcal{I}_{N,t} \triangleq \{j | \mathbb{T}_n(c_j) = \text{I}, c_j \in \mathcal{C}_{N,t}\}$ as the set of information bits corresponding to the PCCMP graph $\mathcal{G}_{N,t}$.
- **Action**: an action a_t is the index of the selected check node that will be set to frozen at time step t . The set of available actions at $s_t = \mathcal{G}_{N,t}$ is $\mathcal{A}(s_t) = \mathcal{I}_{N,t}$.
- **Rules**: the agent interacts with the environment in an episodic manner. To construct $\mathcal{P}(N, K, m)$, each episode starts with a PCCMP graph s_0 with $\mathcal{I}_{N,0} = [N]$. Within an episode, if the agent takes action a_t at state s_t , the state transitions to s_{t+1} , which evolves from s_t by setting $\mathbb{T}_n(c_{a_t}) = \text{F}$. Note that $\mathcal{I}_{N,t+1} = \mathcal{I}_{N,t} \setminus \{a_t\}$.
- **Termination**: an episode terminates in $N - K$ time steps.
- **Reward**: the reward r_{t+1} is designed as the improvement in FER after setting the bit a_t to frozen under CA-SCL decoding. Specifically,

$$r_{t+1} = \log [P_{e,t}(\mathcal{I}_{N,t}, N, m, L, \gamma)] - \log [P_{e,t}(\mathcal{I}_{N,t+1}, N, m, L, \gamma)], \quad (22)$$

where $P_{e,t}(\mathcal{I}_{N,t}, N, m, L, \gamma)$ is the simulated FER at time t of $\mathcal{P}(N, |\mathcal{I}_{N,t}|, m)$ with non-frozen set $\mathcal{I}_{N,t}$ under the CA-SCL decoding with list size L at channel SNR γ .

At the end of each episode, $\mathcal{I}_{N,N-K}$ has exactly K distinct elements in $[N]$, which corresponds to a valid construction for $\mathcal{P}(N, K, m)$. Fig. 3 shows an episode of the agent's interaction with the environment for constructing $\mathcal{P}(4, 2, \cdot)$.

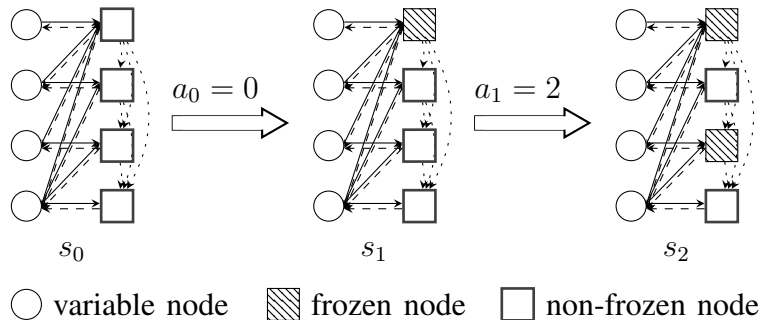


Fig. 3: RL setup of the IMP-based polar-code construction for $\mathcal{P}(4, 2, \cdot)$.

With (22), the cumulative return in each episode with design SNR γ is given by

$$\begin{aligned}
 R &= \sum_{t=0}^{N-K-1} \beta^t r_{t+1} \\
 &= \sum_{t=0}^{N-K-1} \beta^t \left\{ \log [P_{e,t}(\gamma; N, \mathcal{I}_{N,t}, m, L)] - \log [P_{e,t}(\gamma; N, \mathcal{I}_{N,t+1}, m, L)] \right\}. \quad (23)
 \end{aligned}$$

When $\beta = 1$, the expected cumulative return is

$$\mathbb{E}[R] = \sum_{t=0}^{N-K-1} \mathbb{E}[\log [P_{e,t}(\mathcal{I}_{N,t}, N, m, L, \gamma)]] - \mathbb{E}[\log [P_{e,t}(\mathcal{I}_{N,t+1}, N, m, L, \gamma)]] \quad (24)$$

$$= \mathbb{E}[\log [P_{e,0}(\mathcal{I}_{N,0}, N, m, L, \gamma)]] - \mathbb{E}[\log [P_{e,N-K-1}(\mathcal{I}_{N,N-K}, N, m, L, \gamma)]], \quad (25)$$

where (25) follows from $\mathbb{E}[\log [P_{e,t_1}(\mathcal{I}, N, m, L, \gamma)]] = \mathbb{E}[\log [P_{e,t_2}(\mathcal{I}, N, m, L, \gamma)]]$ for any $t_1, t_2 \in [N - K]$. The first term in (25) is determined by the channel condition and the decoding algorithm, and is independent of the agent's policy. Therefore, the policy that maximizes the expected cumulative return automatically minimizes the second term in (25). Equivalently, the policy finds a set of non-frozen bits $\mathcal{I}_{N,N-K}$ that minimizes the FER under the CA-SCL decoding with list size L for the target $\mathcal{P}(N, K, m)$ with design SNR γ .

C. Training Strategies

Since the IMP model design in Section IV-A and the parameter sizes are independent of the PCCMP graph size and code design parameters (N, K, m, γ, L) , the parameters Θ can be trained such that a single IMP model provides good polar codes in various code design scenarios. Note that with the same Θ , the IMP model generates different polar codes for different input parameters N, K , and γ . To learn such parameters Θ , the training can be explicitly performed

on a wide range of input parameters (N, K, γ) . This paper, however, only focuses on the strategy in which the training is conducted across various γ 's with design parameters (N, K, m, L) being constant. Specifically, the design SNR is sampled uniformly at random from range $[\gamma_{\min}, \gamma_{\max}]$ in each training episode. A good selection of range $[\gamma_{\min}, \gamma_{\max}]$ covers or largely overlaps the SNR range of interest and the FER roughly ranges between 10^{-1} and 10^{-5} .

Let Θ^* represent the parameters of the IMP model after training over $[\gamma_{\min}, \gamma_{\max}]$. Denote by $\mathcal{I}(N, K, m, L, \gamma; \Theta^*)$ the non-frozen set identified by this IMP model for $\mathcal{P}(N, K, m)$ at design SNR γ under CA-SCL decoding with list size L . During evaluation, the IMP algorithm provides $\mathcal{I}(N, K, m, L, \gamma_{\text{eval}}; \Theta^*)$ for each evaluation SNR point γ_{eval} . The IMP model trained by this strategy is referred to as ‘‘IMP- $[\gamma_{\min}, \gamma_{\max}]$ -LL’’ in Section V.

To further improve the performance of the trained model for each evaluation SNR, the learned parameters Θ^* are further fine-tuned by feeding a small number of additional training episodes with $\gamma = \gamma_{\text{eval}}$. During evaluation, the construction for each γ_{eval} is given by $\mathcal{I}(N, K, m, L, \gamma_{\text{eval}}; \Theta_{\gamma_{\text{eval}}}^*)$, where $\Theta_{\gamma_{\text{eval}}}^*$ represents the parameter values after fine-tuning at design SNR γ_{eval} . These fine-tuned models are referred to as ‘‘IMP-fine-tuned’’ in Section V.

V. EXPERIMENTAL RESULTS

To evaluate the performance of the IMP algorithm, the FER of the polar code constructed by the IMP algorithm under CA-SCL decoding is compared to that of the polar codes given by the Tal-Vardy's algorithm [8], the RM-Polar method [21], the genetic algorithm (GenAlg) [23], and the tabular RL algorithm [26] for the AWGN channel with QPSK modulation. For each evaluation point, the number of simulated transmissions is such that the number of observed frame errors is at least 500 and the number of total simulated transmissions is at least 10^6 . The hyper-parameters adopted during training and evaluation are specified below.

- 1) **GenAlg** [23]: The hyper-parameters are consistent with the ones adopted in [23]. In particular, the population size is $S = 20$, and the number of truncated parents is $T = 5$ for each population update iteration. The number of Monte-Carlo simulations for the FER estimates in each iteration is set such that either the number of observed frame errors reaches 10^3 or the number of simulated frames reaches 10^6 . The maximum number of population update iterations is $N_{\text{pop,max}} = 1000$. The search and evaluation use the same CA-SCL decoding with the same CRC designs for each evaluation point.

- 2) **Tabular RL method** [26]: The discount rate is set to 1. The trace decay factor λ , the neighborhood update rate κ , and the exploration rate ϵ for the ϵ -greedy policy are initialized as $\lambda = 0.8$, $\kappa = 1$, and $\epsilon = 0.5$, respectively. As the training proceeds, λ , κ , and ϵ are updated gradually toward 0.9, 0, and $\frac{1}{5N}$ for polar codes of length N , respectively. The maximum number of training episodes is 2×10^5 .
- 3) **IMP algorithm**: The maximum message passing iterations M is set to 3. For the initialization operations, the node-type embedding length is $d_{\text{emb}} = 28$ and the initial local-message embedding has length $d_{\text{init}} = 4$, so $d^{(0)} = 32$. The hidden embeddings after each message passing iteration is $d^{(i)} = 64$, $i \in \{1, 2, 3\}$. The global features $\tilde{\mathbf{h}}_c$ and $\tilde{\mathbf{h}}_v$ both have dimension 1. The $\text{POST}(\cdot)$ operation uses a MLP with two hidden layers, each with size 128. The CRC generator polynomial remains constant during training and evaluation. For the reward generation, each FER is estimated by a Monte-Carlo simulation with at most 100 observed frame errors and at most 10^5 frames in total. The DQL algorithm with a replay buffer of size 10^4 and a target Q-value network [31] that updates every 2 episodes is used. During training, the exploration rate is initialized as 0.5, and exponentially decayed to $\frac{1}{5N}$ with 0.999 decay rate. The discount factor β is initialized as 0.8, which increases linearly to 1 in 20 episodes and remains at 1 afterwards.

The rest of this section evaluates the IMP algorithm in three aspects. Specifically, Section V-A shows that the polar codes constructed by the IMP algorithm outperform those constructed by existing methods in many cases; Section V-B verifies the generalization capability of a trained IMP model to different design SNRs and list sizes; and Section V-C illustrates that a trained IMP model can generalize to different blocklengths and still provides good polar codes.

A. Error-Correction Performance

Figs. 4 and 5 compare the FERs of the learned constructions by the IMP algorithm with pointwise fine-tuning to the constructions given by the Tal-Vardy's method [8], the RM-Polar codes² [21], the GenAlg [23], and the tabular RL method [26] for $\mathcal{P}(64, 32, 4)$ and $\mathcal{P}(128, 64, 4)$, respectively. At each γ_{eval} , a polar code tailored for design SNR γ_{eval} is generated by each of the construction methods, and then evaluated by CA-SCL decoding at the same SNR γ_{eval} . Since the

²The RM-Polar construction method is not applicable to $\mathcal{P}(64, 32, 4)$ because there are not enough rows in the generator matrix with high Hamming weights to increase the minimum Hamming distance from the standard construction.

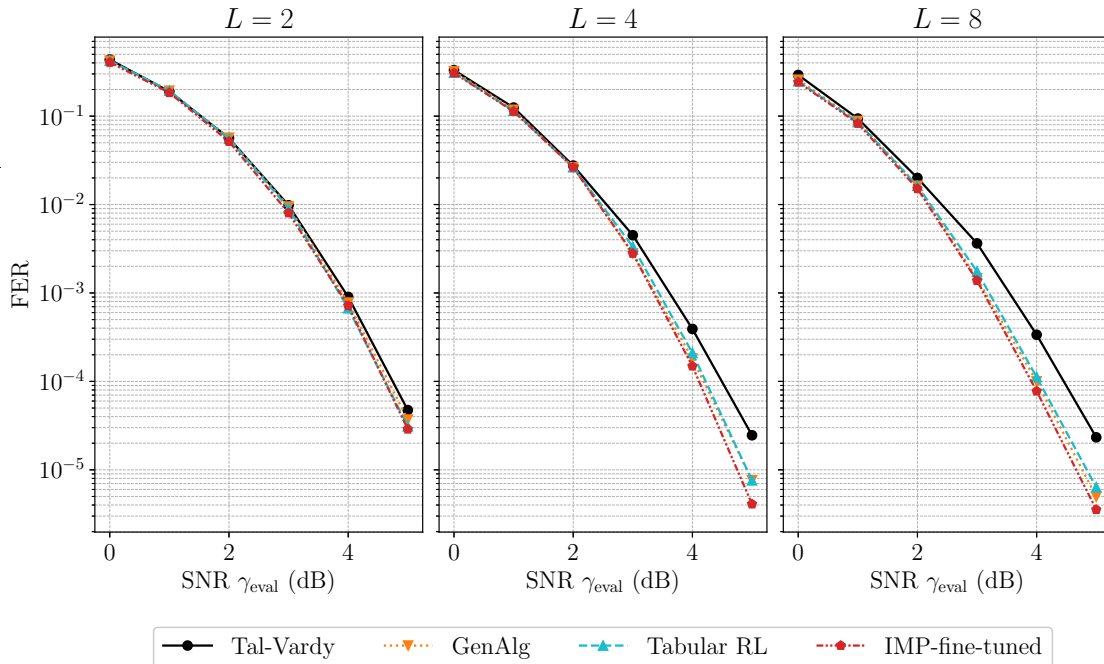


Fig. 4: FERs of $\mathcal{P}(64, 32, 4)$ given by different polar-code construction methods under CA-SCL decoding with list sizes $L = 2$ (left); 4 (middle); 8 (right). The CRC polynomial is 0x3.

constructions are channel-dependent in all considered methods, the polar codes corresponding to different γ_{eval} are potentially different, even when they are generated by the same construction method. The training SNR before fine-tuning is selected uniformly at random from the range $[0, 3.5]$ dB in each episode for $\mathcal{P}(64, 32, 4)$, and the corresponding training SNR range is $[0.5, 3.5]$ dB for $\mathcal{P}(128, 64, 4)$.

As shown in Figs. 4 and 5, the constructions from the IMP-based method consistently outperform the Tal-Vardy's constructions in all evaluated scenarios under CA-SCL decoding with various list sizes L , and the improvement in FER increases with L . This verifies the claim that the polar-code construction methods (e.g., Tal-Vardy's) that target to optimize the error-correction performance for SC decoding can be strictly suboptimal under CA-SCL decoding.

Figs. 4 and 5 also show that the polar codes constructed by the IMP algorithm always achieve the lowest FER among polar codes generated by all existing construction methods tailored for CA-SCL decoding. For a given γ_{eval} and a given decoding list size L , the IMP algorithm finds the same $\mathcal{P}(128, 64, 4)$ as the GenAlg does. We conjecture that the polar codes constructed by these two algorithms are optimal in terms of minimizing FER under the given CA-SCL

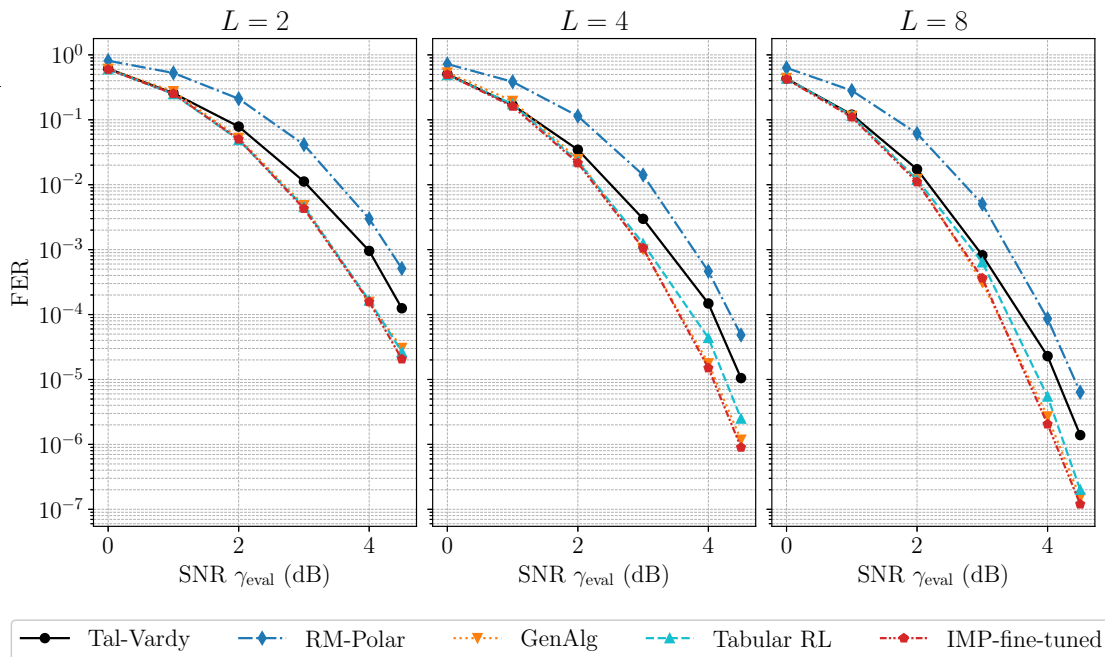


Fig. 5: FERs of $\mathcal{P}(128, 64, 4)$ given by different polar-code construction methods under CA-SCL decoding with list sizes $L = 2$ (left); 4 (middle); 8 (right). The CRC polynomial is 0x3.

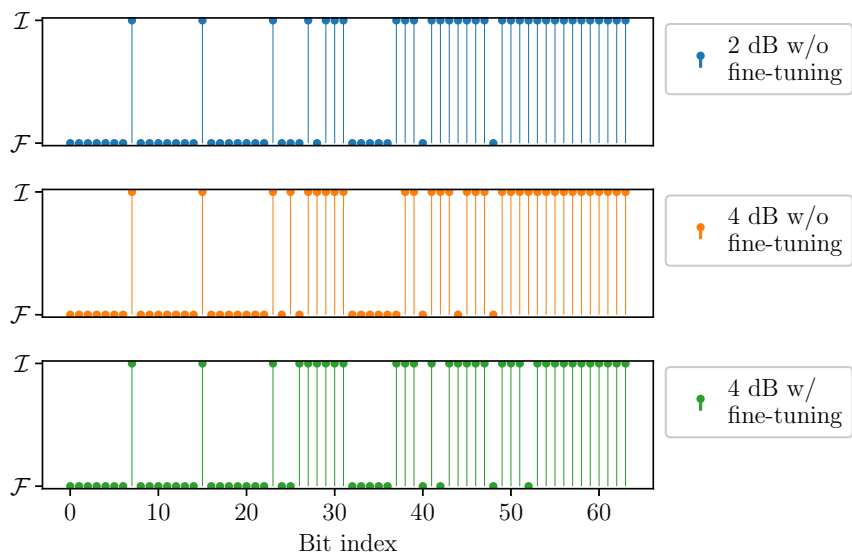
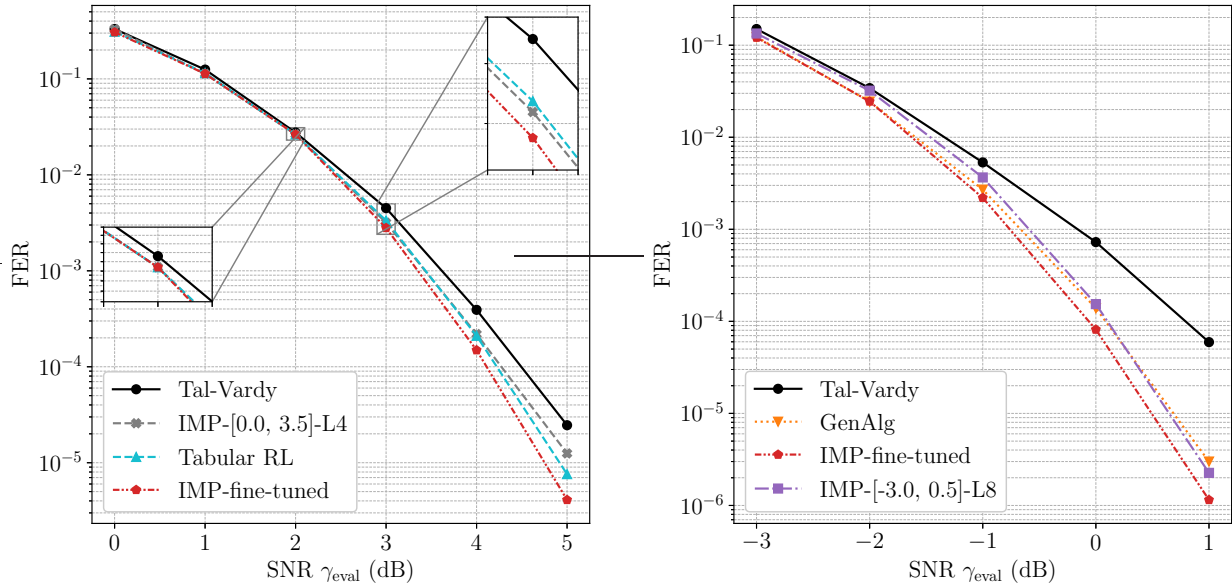


Fig. 6: $\mathcal{P}(64, 32, 4)$ constructed by the “IMP-[0.0, 3.5]-L4” model evaluated at $\gamma_{eval} = 2$ dB (top) and $\gamma_{eval} = 4$ dB (middle), and $\mathcal{P}(64, 32, 4)$ constructed by the “IMP-fine-tuned” model at $\gamma_{eval} = 4$ dB (bottom).



(a) FER of $\mathcal{P}(64, 32, 4)$ under CA-SCL decoding with $L = 4$. The degree-4 CRC polynomial is $0x3$.

(b) FER of $\mathcal{P}(128, 32, 4)$ under CA-SCL decoding with $L = 8$. The degree-4 CRC polynomial is $0x3$.

Fig. 7: Comparison of polar codes constructed by the IMP model with and without fine-tuning.

decoding scheme. When the two algorithms identify the same polar codes at a given γ_{eval} , the IMP algorithm still shows its advantage over the GenAlg algorithm in the sense that the γ_{eval} values that are not seen during training can be directly fed into the same trained IMP model to generate corresponding polar codes. In contrast, the GenAlg model for one given γ_{eval} cannot provide any information about the code construction at any other γ_{eval} .

B. Generalization in Design SNRs and List Sizes

This section illustrates the generalization capability of the IMP model to various design SNRs and to different list sizes without fine-tuning. Note that since γ_{eval} is one of the input features to the IMP model, the same trained IMP model can automatically provide different constructions at different γ_{eval} 's. For example, Fig. 6 shows that the two polar codes generated by the same “IMP-[0.0, 3.5]-L4” model evaluated at $\gamma_{eval} = 2$ dB and $\gamma_{eval} = 4$ dB are distinct.

Fig. 7a shows constructions of $\mathcal{P}(64, 32, 4)$ for CA-SCL decoding with $L = 4$, in which the “IMP-fine-tuned” models use the “IMP-[0.0, 3.5]-L4” model as the starting point of fine tuning. It can be observed that the IMP model trained over the SNR range $[0, 3.5]$ dB without fine-tuning can generate constructions that outperform the Tal-Vardy’s constructions over a large range of

design SNRs, even when γ_{eval} is out of the training SNR range of $[0, 3.5]$ dB. Besides, at some of the evaluation points, e.g., $\gamma_{\text{eval}} = 2$ dB, the IMP model without fine-tuning already finds the same construction as the tabular RL and the fine-tuned model do, while the latter two are trained specifically for that single γ_{eval} point. These observations indicate that the IMP model manages to learn the general rules for constructing polar codes tailored for a given CA-SCL decoder, and the learned rules can be applied to a wide range of design SNRs, even to SNRs outside the training SNR range. On the other hand, Fig. 7a shows that the additional fine-tuning at each evaluation point can effectively improve the learned construction in most cases, especially when the evaluation point is outside the initial training range of the IMP model as evidenced in the bottom two cases in Fig. 6.

Similar observations can be made in Fig. 7b for $\mathcal{P}(128, 32, 4)$ under CA-SCL decoding with $L = 8$. Specifically, the IMP model without fine-tuning outperforms the Tal-Vardy’s method, and fine-tuning can further improve the constructed codes. However, in Fig. 7b, a strictly positive gap is observed between the performance of the trained IMP model over the entire SNR range and the pointwise fine-tuned models, indicating that the trained IMP model is strictly sub-optimal without fine-tuning even within the training SNR range. This gap is mainly caused by the wide training SNR range of $[-3, 0.5]$ dB, in which the FER spans about five orders of magnitude. Due to the wide FER span, the current IMP model fails to generate accurate priority metrics for all training scenarios. This suggests that a more expressive NN architecture is desired for the IMP model if one expects to fit a single IMP model to a SNR range in which the FER spans over a wide range (e.g., several orders of magnitude).

Fig. 8 compares different construction methods for $\mathcal{P}(64, 32, 4)$ under CA-SCL decoding with $L = 8$. The “IMP-[0.0, 3.5]-L8” model is fine tuned to obtain the “IMP-fine-tuned” models. Both “IMP-[0.0, 3.5]-L8” and “IMP-[3.0, 5.0]-L8” models provide constructions that outperform the Tal-Vardy’s constructions in the entire evaluation SNR range, though the improvement is minimal for both models when γ_{eval} is outside the training ranges. Again, fine-tuning helps to find constructions with even lower FERs. It is also observed that the FER curves for the model “IMP-[0, 3.5]-L8” and the model “IMP-[3.0, 5.0]-L8” intersect between 3 dB and 4 dB SNR. This implies that if the IMP model is applied without fine-tuning, better constructions are expected when the design SNR is within the training SNR range.

Fig. 8 also shows the effect of decoding scheme mismatch during training and evaluation. Specifically, under the CA-SCL decoding with $L = 8$, the FER of polar codes constructed by

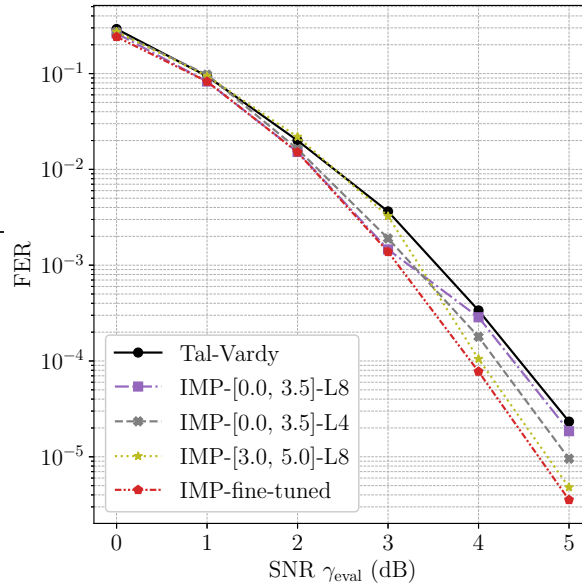


Fig. 8: FER performance of $\mathcal{P}(64, 32, 4)$ given by different polar-code construction methods under CA-SCL decoding with $L = 8$. The degree-4 CRC polynomial is $0x3$.

the “IMP-[0.0, 3.5]-L4” model is contrasted with that of polar codes constructed by the “IMP-[0.0, 3.5]-L8” model. With the same training SNR range, the polar codes constructed by the latter IMP model have lower FER compared to the polar codes constructed by the former one when evaluated within the training SNR range. This suggests that the constructions given by the trained IMP model is effectively tailored for the decoding scheme during training. On the other hand, the codes constructed by the “IMP-[0.0, 3.5]-L4” model show constantly lower FERs than the Tal-Vardy’s constructions under the CA-SCL decoding with $L = 8$, meaning that the IMP models trained for one CA-SCL decoding scheme are likely to provide constructions that are also reasonably good in FER performance under CA-SCL decoding with different list sizes.

C. Generalization in Blocklength N

In Fig. 9, the “IMP-[0.0, 3.5]-L4” model trained on $\mathcal{P}(128, 64, 4)$ is directly applied to construct polar codes with a larger blocklength $N = 1024$. The curve labeled “IMP-[0.0, 3.5]-L4-N128” shows the performance of the polar codes given by the trained IMP model when the input SNR to the model matches the evaluation SNR. Note that such IMP-based polar codes outperform the Tal-Vardy’s constructions and the RM-Polar constructions, and the improvement in FER becomes significant in the high SNR regime.

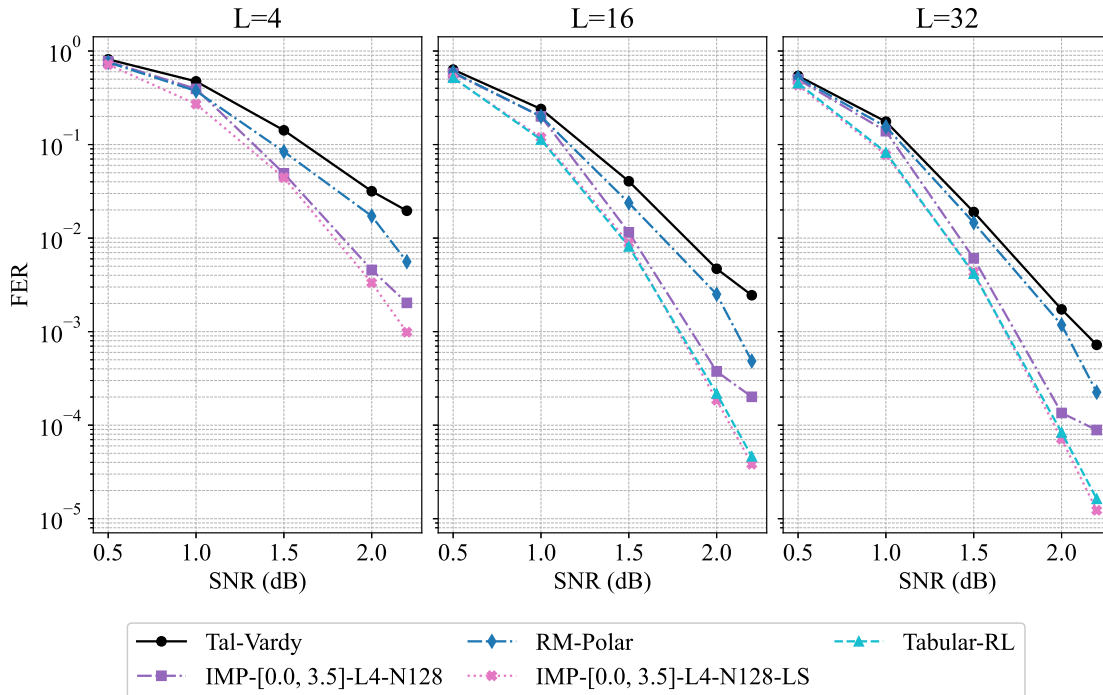


Fig. 9: FER curves of $\mathcal{P}(1024, 512, 32)$ given by different construction algorithms. The CRC polynomial is 0x04C11DB7. Constructions for points on both curves of the IMP algorithm adopt the same IMP model trained for $\mathcal{P}(128, 64, 4)$ under CA-SCL decoding with $L = 4$ without fine-tuning.

Further improvement is obtained by adding an additional neighborhood search (NS) over the input SNRs of the IMP model (the performance is reported in the curve labeled “IMP-[0.0, 3.5]-L4-N128-NS”). In particular, at each evaluation SNR point γ_{eval} , five SNR values $\{\gamma_{\text{eval}}, \gamma_{\text{eval}} \pm 0.2, \gamma_{\text{eval}} \pm 0.4\}$ are fed into the trained IMP model and five candidate constructions are generated. These candidates are then evaluated by the CA-SCL decoding and the construction that achieves the lowest FER is selected as the final construction for the evaluation point γ_{eval} . The performance of the IMP algorithm with neighborhood search is comparable to the tabular RL method, while the latter one requires separate training for every different triple $(N, K, \gamma_{\text{eval}})$. The adopted IMP model, on the other hand, is applied with no additional training on N , K , and γ_{eval} . These observations verify the generalization capability of IMP models to different (N, K, γ) without additional training.

VI. CONCLUSION

This paper investigates the problem of scalable and generalizable construction methods of polar codes tailored for the CA-SCL decoding. A GNN-based IMP algorithm is proposed and described, whose NN model complexity is independent of the target blocklength and code rate, making the algorithm readily scalable to large blocklengths and various target code rates. Experiments verify that the IMP algorithm can successfully find polar-code constructions that significantly outperform the classical constructions under the CA-SCL decoding. Compared to existing polar-code construction methods tailored for CA-SCL decoding, the IMP algorithm can either find constructions that achieve lower FERs or find constructions with similar FER performance with significantly lower training complexity. A salient feature of the IMP algorithm is that a single trained IMP model can be directly applied to provide constructions for various design SNRs and different blocklengths without any additional training. This feature makes the IMP algorithm a powerful candidate in real-world deployment, in which the wireless channel condition varies over time and searching for good polar codes for each design requirement separately can be complicated and costly.

The IMP algorithm illustrated the potential of using GNN as a tool for code design problems. Some future research directions using similar methods may include: (a) polar-code constructions on different channels such as fading channels; (b) variations of the graph structures, e.g., different connection patterns among check nodes; (c) graph-based algorithms that enable joint learning over non-frozen set and CRC design; and (d) GNN-based code designs tailored for BP decoding and other decoding algorithms.

APPENDIX I

SPECIAL CASES OF THE IMP ALGORITHM

This appendix shows an example on how the conventional polar-code construction methods tailored for the SC decoding can be mapped to the IMP algorithm. The example only showcases a feasible view of the conventional methods from the graph-based perspective, and can be far from optimal in terms of the complexity of the message processing functions $\text{INIT}(\cdot)$, $\text{AGG}(\cdot)$, $\text{UP}(\cdot)$, $\text{POST}(\cdot)$, etc. CRC is commonly not considered in the code constructions for SC decoding, so the notation of a polar code with length N and rate K/N is simplified as $\mathcal{P}(N, K)$ throughout the appendix.

Algorithm 2 Abstraction of Classical Polar-Code Construction Algorithms

Input: N , K , design channel parameter γ .

Output: frozen set \mathcal{F} and non-frozen set \mathcal{I}

- 1: $n \leftarrow \log_2 N$
 - 2: Create data structure \mathbf{Z} with $n + 1$ rows, in which row l has 2^l elements, $l \in \{0, \dots, n\}$.
 - 3: Initialize the first row of \mathbf{Z} by $Z[0, 0] \leftarrow F_{\text{init}}(\gamma; N, K)$.
 - 4: **for** $l \leftarrow 0 : n - 1$ **do**
 - 5: Offset $\Delta_l \leftarrow 2^l$.
 - 6: **for** $t \leftarrow 0 : \Delta_l - 1$ **do**
 - 7: $Z[l + 1, t] \leftarrow F_{\text{left}}(Z[l, t])$
 - 8: $Z[l + 1, t + \Delta_l] \leftarrow F_{\text{right}}(Z[l, t])$
 - 9: **end for**
 - 10: **end for**
 - 11: Compute the final metric vector $\mathbf{z}^* \in \mathbb{R}^N$ by $z^*[t] \leftarrow F_{\text{post}}(Z[n, t])$.
 - 12: \mathcal{F} is constructed as the set of indices of the largest $N - K$ elements in \mathbf{z}^* , and $\mathcal{I} \leftarrow [N] \setminus \mathcal{F}$.
-

A. Abstraction of Classic Polar-Code Construction Algorithm

Algorithm 2 provides an abstraction of many classical construction methods tailored for SC decoding that are based on the channel polarization and bit-channel reliability estimation. Different instantiations of the initialization operation F_{init} , the left-branch operation F_{left} , the right-branch operation F_{right} , and a post-processing operation F_{post} , as well as different choices of the channel parameters γ result in different estimates of the bit-channel reliability. The variable \mathbf{Z} in Algorithm 2 is a step-shaped data structure. For constructing polar codes with length $N = 2^n$, \mathbf{Z} has $n + 1$ rows with indices in $[0, 1, \dots, n]$, in which the row with index l is a vector of length 2^l . $Z[l, t]$ denote the entry at column t and row l . Both indices start from 0.

An example is the Gaussian approximation method in [7] for polar-code construction in the binary-input AWGN (BI-AWGN) channels, in which the operations in Algorithm 2 can be instantiated as $F_{\text{init}} = 4\gamma$ (dB), $F_{\text{left}}(x) = \phi^{-1}(1 - (1 - \phi(x))^2)$, $F_{\text{right}}(x) = 2x$, and $F_{\text{post}}(x) = -x$, where the interpolation function ϕ can be found in [7].

B. IMP Algorithm for the SC Decoding

The bit-channel reliability estimates that can be abstracted in Algorithm 2 are independent of whether the bits are frozen or non-frozen. Therefore, it is expected that the equivalent IMP for these algorithms do not distinguish non-frozen and frozen check nodes in their initial embeddings, and the priority metrics z calculated in each of the $N - K$ steps remain the same. This section presents a simplified IMP algorithm tailored for the SC decoding that utilizes $\{F_{\text{init}}, F_{\text{left}}, F_{\text{right}}, F_{\text{post}}\}$ from Algorithm 2 in the operation designs. The operations F_{left} and F_{right} are defined over extended domains that include $\{-\infty\}$, where $F_{\text{left}}(-\infty) = F_{\text{right}}(-\infty) = -\infty$.

Consider an IMP algorithm on the PCCMP graph \mathcal{G}_N , in which the hidden embedding $\mathbf{h}_u^{(i)} \in \mathbb{R}^{2N}$ at each node $u \in \mathcal{V}_N$ after each message passing iterations. The initial node features and IMP operations are designed as follows.

- **Initial messages at each node:**

$$x_u = \begin{cases} \gamma, & \mathbb{T}_n(u) = V, \\ j, & u = c_j. \end{cases} \quad (26)$$

- **Initialization:**

$$\mathbf{h}_{c_j}^{(0)} = \text{INIT}_{\mathbb{T}_n(c_j)}(x_{c_j}) = \text{INIT}_{\mathbb{T}_n(c_j)}(j) = [j, -\infty \cdot \mathbf{1}_{2N-1}^\top]^\top, \quad j \in [N], \quad (27)$$

$$\mathbf{h}_{v_j}^{(0)} = \text{INIT}_V(x_{v_j}) = \text{INIT}_V(\gamma) = [\gamma, F_{\text{init}}(\gamma; N, K), -\infty \cdot \mathbf{1}_{2N-2}^\top]^\top, \quad j \in [N], \quad (28)$$

where $\mathbf{1}_l$ represents an all-ones column vector of length l .

- **Aggregation operations:** the max-pooling operation MAXPOOL is adopted by all aggregation operations $\text{AGG}_{\text{mt}}^{(i)}$ and local aggregation operations $\text{AGG}^{(i)}$. Formally, the max-pooling operation over a set of length- l vectors $\{\mathbf{h}_w\}_{w \in \mathcal{N}}$ is defined as

$$\text{MAXPOOL}(\{\mathbf{h}_w\}_{w \in \mathcal{N}}) \triangleq \left[\max\{h_w[0] | w \in \mathcal{N}\}, \dots, \max\{h_w[l-1] | w \in \mathcal{N}\} \right]^\top. \quad (29)$$

- **Update operations:** the update operations $\text{UP}_{c2c}^{(i)}$ and $\text{UP}_{v2c}^{(i)}$ that affect check nodes' embeddings take the same format as

$$\mathbf{y} = \text{UP}_{c2c}^{(i)}(\mathbf{h}, \mathbf{h}_{\mathcal{N}}) = \text{UP}_{v2c}^{(i)}(\mathbf{h}, \mathbf{h}_{\mathcal{N}}) \triangleq \left[h[0], \tilde{F}_{\text{left}}(\bar{\mathbf{h}})^\top \right]^\top, \quad (30)$$

where $\bar{\mathbf{h}} = \text{MAXPOOL}(\{\mathbf{h}, \mathbf{h}_{\mathcal{N}}\})$ and $\tilde{F}_{\text{left}}(\bar{\mathbf{h}})$ calculates $y[1], y[2], \dots, y[2N-1]$ in accordance with

$$y[k] = \begin{cases} F_{\text{left}}(\bar{h}[k']), & \text{if } \bar{h}[k] = -\infty, \exists k' \in \mathbb{Z}_+, \text{ s.t. } k = k' + 2^{\lfloor \log_2(k') \rfloor}. \\ \bar{h}[k], & \text{otherwise.} \end{cases} \quad (31)$$

Similarly, the update operations $\text{UP}_{c_{2v}}^{(i)}$ are set to

$$\mathbf{y} = \text{UP}_{c_{2v}}^{(i)}(\mathbf{h}, \mathbf{h}_{\mathcal{N}}) \triangleq \left[h[0], \tilde{F}_{\text{right}}(\bar{\mathbf{h}})^\top \right]^\top, \quad (32)$$

where $\bar{\mathbf{h}} = \text{MAXPOOL}(\{\mathbf{h}, \mathbf{h}_{\mathcal{N}}\})$ and $\tilde{F}_{\text{right}}(\bar{\mathbf{h}})$ calculates $y[1], y[2], \dots, y[2N-1]$ in accordance with

$$y[k] = \begin{cases} F_{\text{right}}(\bar{h}[k']), & \text{if } \bar{h}[k] = -\infty, \exists k' \in \mathbb{Z}_+, \text{ s.t. } k = k' + 2^{\lfloor \log_2(k') \rfloor + 1}, \\ \bar{h}[k], & \text{otherwise.} \end{cases} \quad (33)$$

- **Post-processing operations:** the post-processing operation at check node c_j is

$$\text{POST}(\mathbf{h}_{c_j}^{(M)}) = F_{\text{post}}\left(h_{c_j}^{(M)} \left[N + h_{c_j}^{(M)}[0] \right]\right). \quad (34)$$

Note that the index $N + h_{c_j}^{(M)}[0]$ in (34) is valid. Since the update operations $\text{UP}_{\text{mt}}^{(i)}(\mathbf{h}_u, \mathbf{h}_{\mathcal{N}})$ defined in (30) and (32) keep the same local $h_u[0]$ as the first element in the resulting embedding for every mt, all inputs to the local aggregation operation $\text{AGG}^{(i)}$ at u contain the same first element $h_u[0]$. Therefore, $h_u[0]$ is carried over to the next iteration after $\text{AGG}^{(i)}$ for every i . This implies $h_u^{(M)}[0] = h_u^{(M-1)}[0] = \dots = h_u^{(0)}[0]$ for all nodes u . In particular, for the check node c_j , $h_{c_j}^{(M)}[0] = j$, and the index $N + h_{c_j}^{(M)}[0]$ in (34) is simply $N + j \in [2N]$.

C. Equivalence of the IMP Algorithm and Algorithm 2 for the SC Decoding

The equivalence between the IMP model specified in Appendix I-B and the construction method in Algorithm 2 becomes clear when the operations on \mathbf{h} are translated to operations on the corresponding \mathbf{Z} structures. Define the vector

$$\mathbf{h}^* \triangleq \left[-\infty, \text{vec}(\mathbf{Z}^*)^\top \right]^\top \in \mathbb{R}^{2N}, \quad (35)$$

where $\text{vec}(\mathbf{Z}^*)$ is the flattened version of the data structure \mathbf{Z} at the end of Algorithm 2, in which $Z^*[l, t] = h^*[2^l + t]$ for all $l \in [n]$, $t \in [2^l]$.

Claim 1: If a construction method fits into Algorithm 2 by a set of operations $\{F_{\text{init}}, F_{\text{left}}, F_{\text{right}}, F_{\text{post}}\}$, the IMP algorithm with the parameters and operations specified in Appendix I-B reproduces the data structure \mathbf{Z}^* and picks the same \mathcal{F} given by that construction method.

Proof: The proof follows from the key observation that $h_u^{(i)}[k] \in \{-\infty, h^*[k]\}$ for all $u \in \mathcal{V}_N$, $k \in \{1, 2, \dots, 2N - 1\}$, and $i \in [M]$. This observation can be verified by induction on i (where the base case is determined by F_{init}), and by the equivalence of (30) and (32) on the hidden embeddings to F_{left} and F_{right} operations on the \mathbf{Z} data structure, respectively. Then, it follows that the number of finite entries in $\mathbf{h}_u^{(i)}$ is strictly increasing in every two message passing iterations until all entries in $\mathbf{h}_u^{(i)}$ are filled with finite values. This implies that $h_u^{(i)}[k] = h^*[k]$ for all $i \geq 2N + 1$, i.e., \mathbf{Z}^* can be recovered at all nodes $u \in \mathcal{V}_N$ in at most $2N + 1$ message passing iterations. The post processing (34) returns $F_{\text{post}}(h^*[N + j]) = F_{\text{post}}(\mathbf{Z}^*[n, j]) = z^*[j]$ at check node c_j , which matches the final metric in Algorithm 2. Therefore, the frozen set \mathcal{F} constructed with the IMP algorithm in Appendix I-B matches the output \mathcal{F} of Algorithm 2. ■

REFERENCES

- [1] E. Arkan, "Channel polarization: A method for constructing capacity-achieving codes for symmetric binary-input memoryless channels," vol. 55, no. 7, pp. 3051–3073, 2009.
- [2] 3GPP, "Final report of 3GPP TSG RAN WG1 #87 v1.0.0," Reno, USA, Nov. 2016.
- [3] I. Tal and A. Vardy, "List decoding of polar codes," *IEEE Trans. Inf. Theory*, vol. 61, no. 5, pp. 2213–2226, 2015.
- [4] H. Li and J. Yuan, "A practical construction method for polar codes in awgn channels," in *IEEE 2013 Tencon-Spring*. IEEE, 2013, pp. 223–226.
- [5] R. Mori and T. Tanaka, "Performance and construction of polar codes on symmetric binary-input memoryless channels," in *2009 IEEE Int. Sym. Inf. Theory (ISIT)*, 2009, pp. 1496–1500.
- [6] —, "Performance of polar codes with the construction using density evolution," *IEEE Commun. Lett.*, vol. 13, no. 7, pp. 519–521, 2009.
- [7] P. Trifonov, "Efficient design and decoding of polar codes," *IEEE Trans. Commun.*, vol. 60, no. 11, pp. 3221–3227, 2012.
- [8] I. Tal and A. Vardy, "How to construct polar codes," *IEEE Trans. Inf. Theory*, vol. 59, no. 10, pp. 6562–6582, 2013.
- [9] S. Sun and Z. Zhang, "Designing practical polar codes using simulation-based bit selection," *IEEE J. Emerging and Sel. Topics in Circuits and Syst.*, vol. 7, no. 4, pp. 594–603, 2017.
- [10] M. Bardet, V. Dragoi, A. Otmani, and J. Tillich, "Algebraic properties of polar codes from a new polynomial formalism," in *2016 IEEE Int. Sym. Inf. Theory (ISIT)*, 2016, pp. 230–234.
- [11] C. Schürch, "A partial order for the synthesized channels of a polar code," in *2016 IEEE Int. Sym. Inf. Theory (ISIT)*, 2016, pp. 220–224.
- [12] M. Mondelli, S. H. Hassani, and R. L. Urbanke, "Construction of polar codes with sublinear complexity," *IEEE Trans. Inf. Theory*, vol. 65, no. 5, pp. 2782–2791, 2019.

- [13] G. He, J. Belfiore, I. Land, G. Yang, X. Liu, Y. Chen, R. Li, J. Wang, Y. Ge, R. Zhang, and W. Tong, "Beta-expansion: A theoretical framework for fast and recursive construction of polar codes," in *2017 IEEE Global Commun. Conf. (GLOBECOM)*, 2017, pp. 1–6.
- [14] M. Mondelli, S. H. Hassani, and R. L. Urbanke, "From polar to Reed-Muller codes: A technique to improve the finite-length performance," *IEEE Trans. Commun.*, vol. 62, no. 9, pp. 3084–3091, 2014.
- [15] H. Yao, A. Fazeli, and A. Vardy, "A deterministic algorithm for computing the weight distribution of polar codes," in *2021 IEEE Int. Sym. Inf. Theory (ISIT)*, 2021, pp. 1218–1223.
- [16] M. C. Coşkun and H. D. Pfister, "An information-theoretic perspective on successive cancellation list decoding and polar code design," *IEEE Trans. Inf. Theory*, pp. 1–1, 2022, early access.
- [17] T. Wang, D. Qu, and T. Jiang, "Parity-check-concatenated polar codes," *IEEE Commun. Lett.*, vol. 20, no. 12, pp. 2342–2345, 2016.
- [18] H. Zhang, R. Li, J. Wang, S. Dai, G. Zhang, Y. Chen, H. Luo, and J. Wang, "Parity-check polar coding for 5G and beyond," in *2018 IEEE Int. Conf. Commun. (ICC)*, 2018, pp. 1–7.
- [19] P. Trifonov and V. Miloslavskaya, "Polar subcodes," *IEEE J. Select. Areas Commun.*, vol. 34, no. 2, pp. 254–266, 2015.
- [20] M. Qin, J. Guo, A. Bhatia, A. Guillén i Fàbregas, and P. H. Siegel, "Polar code constructions based on LLR evolution," *IEEE Commun. Lett.*, vol. 21, no. 6, pp. 1221–1224, 2017.
- [21] B. Li, H. Shen, and D. Tse, "A RM-polar codes," 2014.
- [22] P. Yuan, T. Prinz, G. Böcherer, O. Iscan, R. Boehnke, and W. Xu, "Polar code construction for list decoding," in *VDE 12th Int. ITG Conf. Syst., Commun. and Coding*, 2019, pp. 1–6.
- [23] A. Elkelesh, M. Ebada, S. Cammerer, and S. ten Brink, "Decoder-tailored polar code design using the genetic algorithm," *IEEE Trans. Commun.*, vol. 67, no. 7, pp. 4521–4534, 2019.
- [24] L. Huang, H. Zhang, R. Li, Y. Ge, and J. Wang, "AI coding: Learning to construct error correction codes," *IEEE Trans. Commun.*, vol. 68, no. 1, pp. 26–39, 2020.
- [25] M. Ebada, S. Cammerer, A. Elkelesh, and S. ten Brink, "Deep learning-based polar code design," in *IEEE 57th Annual Allerton Conf. Commun., Control, and Computing (Allerton)*, 2019, pp. 177–183.
- [26] Y. Liao, S. A. Hashemi, J. M. Cioffi, and A. Goldsmith, "Construction of polar codes with reinforcement learning," *IEEE Trans. Commun.*, vol. 70, no. 1, pp. 185–198, 2022.
- [27] W. L. Hamilton, "Graph representation learning," *Synthesis Lectures on Artificial Intelligence and Machine Learning*, vol. 14, no. 3, pp. 1–159, Sept. 2020.
- [28] J. Gilmer, S. S. Schoenholz, P. F. Riley, O. Vinyals, and G. E. Dahl, "Neural message passing for quantum chemistry," in *Int. Conf. Machine Learning*. PMLR, July 2017, pp. 1263–1272.
- [29] C. Zhang, D. Song, C. Huang, A. Swami, and N. V. Chawla, "Heterogeneous graph neural network," in *Proc. the 25th ACM SIGKDD Int. Conf. Knowledge Discovery & Data Mining*, 2019, pp. 793–803.
- [30] W. Hamilton, Z. Ying, and J. Leskovec, "Inductive representation learning on large graphs," *Adv. in Neural Inf. Process. Syst.*, vol. 30, 2017.
- [31] V. Mnih, K. Kavukcuoglu, D. Silver, A. Graves, I. Antonoglou, D. Wierstra, and M. Riedmiller, "Playing atari with deep reinforcement learning," *arXiv preprint arXiv:1312.5602*, 2013.